Materials Science and Engineering, 57 (1983) 113–126

The Effect of Polycrystallinity on the Shock Wave Response of Fe–34.5wt.%Ni and Fe–15wt.%Cr–15wt.%Ni

MARC A. MEYERS

Department of Metallurgical and Materials Engineering, New Mexico Institute of Mining and Technology, Socorro, NM 87801 (U.S.A.)

L. E. MURR

Oregon Graduate Center, Beaverton, OR 97006 (U.S.A.)

C. Y. HSU

Department of Materials Science and Engineering, Massachusetts Institute of Technology, Cambridge, MA 02139 (U.S.A.)

G. A. STONE

Department of Metallurgical Engineering, South Dakota School of Mines and Technology, Rapid City, SD 57701 (U.S.A.)

(Received May 14, 1982; in revised form July 9, 1982)

SUMMARY

The effect of polycrystallinity on the shock wave response of Fe–34.5wt.%Ni and Fe–15wt.%Cr–15wt.%Ni alloys was studied by subjecting monocrystalline and polycrystalline cylinders to a normal shock pulse having a peak pressure of 7.5 GPa, a pulse duration of 1.2 μs and an average rarefaction rate of 100 GPa μs^{-1}. No systematic difference in the rate of decay of hardness as a function of the distance from the impact surface could be found between the monocrystalline and polycrystalline specimens. This indicates that, at the pressure and within the total depth investigated, polycrystallinity does not have a noticeable effect on the attenuation of the shock pulse. Transmission electron microscopy yielded results consistent with the hardness measurements. The dislocation substructures consisted of mainly irregular tangles for Fe–34.5wt.%Ni and of planar arrays for Fe–15wt.%Cr–15wt.%Ni, as expected from the higher stacking fault energy of Fe–34.5wt.%Ni.

The shock-loaded Fe–34.5wt.%Ni bicrystal exhibited work softening on subsequent deformation in tensile testing. The work softening was responsible for the abnormal "bulging-out" of the material under the hardness indentations, obscuring the results.

1. INTRODUCTION

Both shock wave parameters (pressure [1], pulse duration [2] and rarefaction rate [3]) and material parameters (grain size [4, 5], stacking fault energy [6] etc.) can affect the residual structure and properties of shock-loaded metals. The rate at which the energy of the shock wave is deposed in the material in the form of dissipative processes (heat and defect generation) should determine its attenuation rate; the greater the energy deposed, the greater is the attenuation rate. Experimental measurements made by Rempel *et al.* [7] and Erkman and Christensen [8] showed that the actual attenuation of a shock wave is different from predictions based on hydrodynamic calculations, which assume that the material has a shear modulus equal to zero and that no defects are generated. Calculations by Meyers and Carvalho [9] suggested that a shock wave traveling in a polycrystalline medium would not have a planar front because of the anisotropy of the individual grains; consequently a "wavy" wave front would result; the dispersion of the wave front in polycrystalline metals should contribute to a higher attenuation rate.

In an effort to investigate whether the grain boundaries and different crystallographic

0025-5416/83/0000-0000/$03.00

orientations in polycrystalline materials have an effect on the rate of attenuation of a shock wave an experiment was devised to compare the residual properties of two monocrystalline and polycrystalline alloys. The choice of Fe-34wt.%Ni and Fe-15wt.%Cr-15wt.%Ni was dictated by three reasons: (a) they have stacking fault energies that are substantially different, resulting in different post-shock structure and properties; (b) their response to conventional deformation has been fully characterized in previous studies [10–12]; (c) they were readily available. Both are single-phase f.c.c. alloys; the stacking fault energy of Fe-15wt.%Cr-15wt.%Ni is considerably lower than that of Fe-34wt.%Ni. The results of this investigation are described in the following sections.

2. EXPERIMENTAL PROCEDURES

The alloys were prepared at the Advanced Materials Research and Development Laboratory, Pratt and Whitney Aircraft, in the form of cylinders 32 mm in diameter and 160 mm in length. The Fe-15wt.%Cr-15wt.%Ni cylinder was a monocrystal and the Fe-34.5wt.%Ni was a bicrystal with a grain boundary along the axis of the cylinder. The orientations are discussed later. The crystals intended for the production of polycrystal were homogenized for 48 h at 1100 K in a protective salt bath (15%–25% NaCl, 20%–32% KCl and 50%–60% BaCl). Polycrystals were made from the monocrystals and bicrystals by cutting discs 50 mm long from the cylinders and homogeneous upsetting in a Tinius-Olsen universal testing machine to a strain of −0.20 at ambient temperature. Microstructural observation of small samples removed from the disc revealed incomplete recrystallization, after a heat treatment of 1070 K for 1 h. This indicated the necessity of further upsetting, which was conducted after the discs had been preheated to 470 K in a muffle furnace. The reason for the preheating was to avoid cracking in the cylinders during deformation. In the second schedule the discs were reduced by a strain of −0.35. The upsetting was conducted by lubricating the platen-disc interface; the extent of barreling was not excessive, but the anisotropy of strain reflective of the anisotropic mechanical properties of the crystals could be clearly observed. After a recrystallization treatment of 1 h at 1070 K, the discs were truly polycrystalline. The grain size, determined by the mean linear intercept, was the same for both alloys: 20 μm. The polycrystal, bicrystal and monocrystal were then machined in order to be mounted into the experimental set-up shown in Fig. 1. The monocrystal (Fe-15wt.%Cr-15wt.%Ni) and bicrystal (Fe-34.5wt.%Ni) were only homogenized after being machined, to eliminate any possible effect of the deformation during machining; it is known that dislocations can travel substantial distances in monocrystals, and dislocations are inevitably generated at the surface. The single crystals were chemically polished after machining (prior to homogenizing) in order to remove the deformed surface layer.

The experimental set-up used for shock loading is shown in Fig. 1. All components (except the screws) are AISI 304 stainless steel. This alloy is austenitic and has a shock impedance that closely matches that of Fe-34.5wt.%Ni and Fe-15wt.%Cr-15wt.%Ni, minimizing internal reflections. Because a low

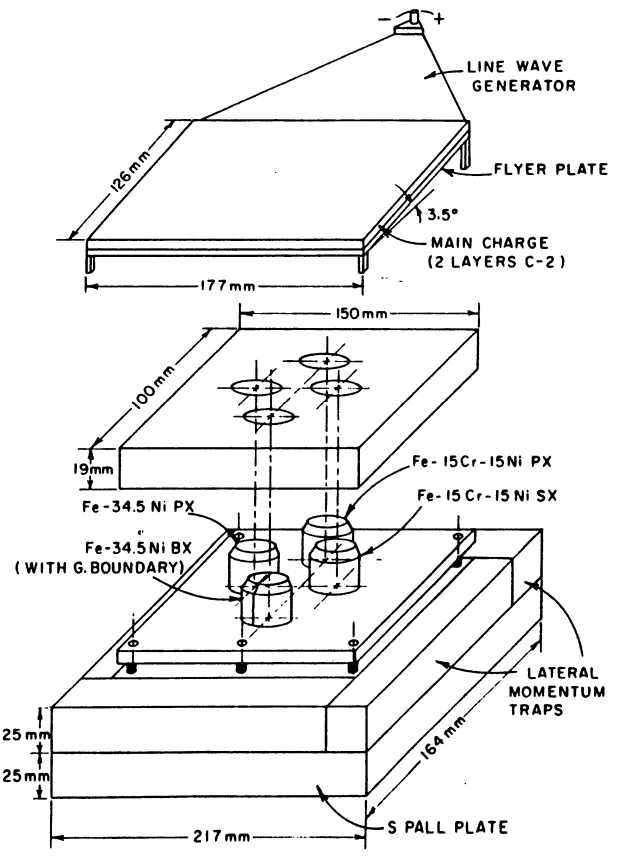

Fig. 1. Set-up to shock load cylindrical specimens: SX, single crystal; BX, bicrystal; PX, polycrystal.

pressure was desired to accentuate the differences in response that might exist between the samples, the inclined-plate set-up was used. The calculations for pressure, pulse duration, rarefaction rate and system dimensions were conducted according to procedures described by deCarli and Meyers [13]. The thickness of the AISI 304 stainless steel driver plate was 3.1 mm and it was inclined with respect to the system with an angle of 3.5°. Two sheets of Datasheet C-2 explosive were used as the main charge; a triangular line wave generator was responsible for transmitting the detonation from the booster charge to the main charge. The stand-off distance (the separation between the system and the driver plate) was equal to 10 mm at the side opposite to the line wave generator and 17.5 mm on the side of the line wave generator. The 45° angle at the top of the discs had the purpose of solidly casing them into the AISI 304 stainless steel block, once the bottom plate had been bolted to it. Lateral bars and a spall plate at the bottom were used to trap the reflected tensile waves. The system was fired into a water tank for rapid cooling and deceleration. The shock wave parameters in the initial stages of propagation were, as calculated using the technique of deCarli and Meyers [13] and Hugoniot data from Kinslow [14], for AISI 304 stainless steel as follows: pressure, 7.5 GPa; pulse duration, 1.2 μs; mean rarefaction rate, 100 GPa μs^{-1}. It should be emphasized that these parameters are slightly different for the Fe-15wt.%Ni-15wt.%Cr and Fe-34.5wt.%Ni alloys because of their slightly different compositions, resulting in different Hugoniot curves. However, the differences are not so great as to warrant separate calculations.

The crystallographic orientation of the crystals was determined by the back-reflection Laue technique, with the X-ray beam incident to the lateral face of the discs and perpendicular to the cylinder axis. It is shown in Fig. 2 for the Fe-34.5wt.%Ni bicrystal. The top surface of the disc (parallel to the plane of the shock front) is marked TOP. Two exposures were made, one on each side of the boundary shown schematically in Fig. 1. The boundary was rendered visible by an appropriate etch. Grain 1 and grain 2 are shown in the stereographic projection. The angle between the (001) of the two grains is 19.5° and the boundary divides the cylinder, as shown in Fig. 1; its intersection with the top surface is

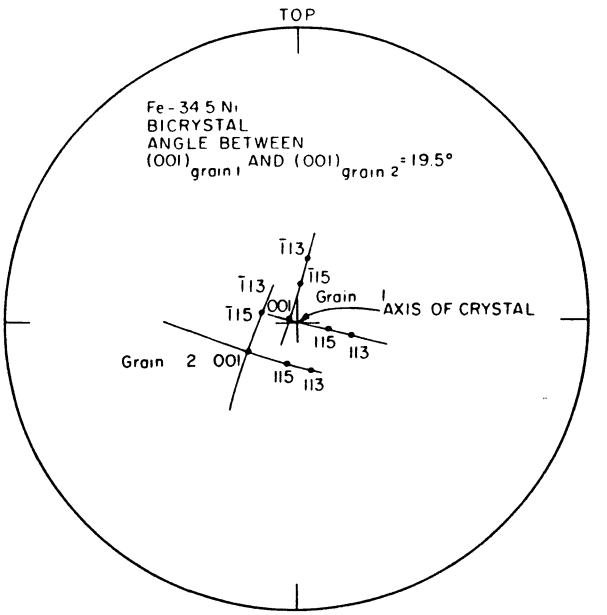

Fig. 2. Crystallographic orientation of two grains in an Fe-34.5wt.%Ni bicrystal. It can be seen that the angle between the two grains is 19.5°.

an irregular line, while its trace on the lateral surface of the cylinder is a straight line, forming an angle of approximately 10° with the cylinder axis. While for one of the grains the top surface of the cylinder is fairly close to (100), for the other it is closer to (110). The slip trace determinations discussed later (see Figs. 5 and 6) refer to the (100) grain, while transmission electron microscopy was done on the (110) grain. The orientation of the top surface of the Fe-15wt.%Cr-15wt.%Ni monocrystal was obtained likewise and was found to be close to (100).

Hardness measurements were made with a diamond pyramid (HDP) indenter using loads of 5 and 10 kgf. Because there were slight variations in hardness when different weights were used, the loads will always be specified. Pre-shock measurements were made on the top and bottom surfaces of the discs and were essentially the same; post-shock hardness measurements were made on the sides, in addition to the top and bottom. For the measurements on the sides, lateral platforms were made by grinding the sides; two platforms were made for each disc. All the hardness measurements are the averages of ten or more readings, and the standard deviations were determined and are marked in the plots. Tensile tests were conducted in an Instron model

1122 operated at a velocity providing a strain rate of $2 \times 10^{-4} s^{-1}$. The specimens were made by sawing discs 1 mm thick from the cylinder using an Isomet diamond saw and polishing them. The specimens were shoulderless, but the result presented refers to a specimen where necking took place in the central region of the gauge length.

The determination of the indentation diameter as a function of applied load was conducted using a spherical (Rockwell B) indenter with a diameter of 1.6 mm. The indenter was attached to the cross-head of the Instron model 1122 universal testing machine moving at a velocity of $0.5\,mm\,s^{-1}$. The load was increased, initially in 190 N intervals and then in 220 N intervals, up to 3 kN. The diameter of the impression was measured at each step using a Unitron TMS 6967 optical microscope with a stage with micrometer attachment. After a load of approximately 300 N, the same indentation was sequentially loaded.

The deformation produced under a hardness indentation was observed by making an indentation with a Brale (Rockwell C) indenter (a cone with a 120° angle) and cutting the specimen perpendicular to the original surface, so that the new surface intersected the indentation. The slip markings were revealed by chemical polishing in a solution containing 80% H_2O_2, 5% HF and 15% H_2O and were observed under polarized light.

Transmission electron microscopy was conducted on foils that were parallel to the top surface of the discs. The foils were prepared by cutting a thin slice (0.31 mm thick) of the disc, after a 1 mm layer had been removed from the bottom and from the top with an Isomet diamond blade. The bottom and top layers were avoided because of heating, wave interaction or other possible surface effects. The slices were then reduced to approximately 0.1 mm by mechanical polishing using grade 0000 paper. Subsequently, 3 mm discs were punched out of the foils and were electropolished in a Fishione twin-jet electropolisher using a solution of 90% acetic acid and 10% perchloric acid at an operating current of 20 mA and a temperature of 298 K. The electron-transparent discs were observed in an Hitachi HU 200 F transmission electron microscope operated at 200 kV, employing a goniometer tilt stage and double-condenser beam illumination.

3. RESULTS AND DISCUSSION

Figures 3 and 4 show the post-shock hardnesses of the four specimens as a function of the distance from the top surface. As expected, the hardness is a maximum in the proximity of the top surface and decreases as the wave attenuates itself in the downward trajectory. The pre-shock hardnesses are indicated in the same plot. However, it should be noted that the correlation between post-shock hardnesses on the top and bottom surfaces and on the lateral platforms is rather poor. Table 1 gives the pre- and post-shock hardness measurements made on the top and bottom

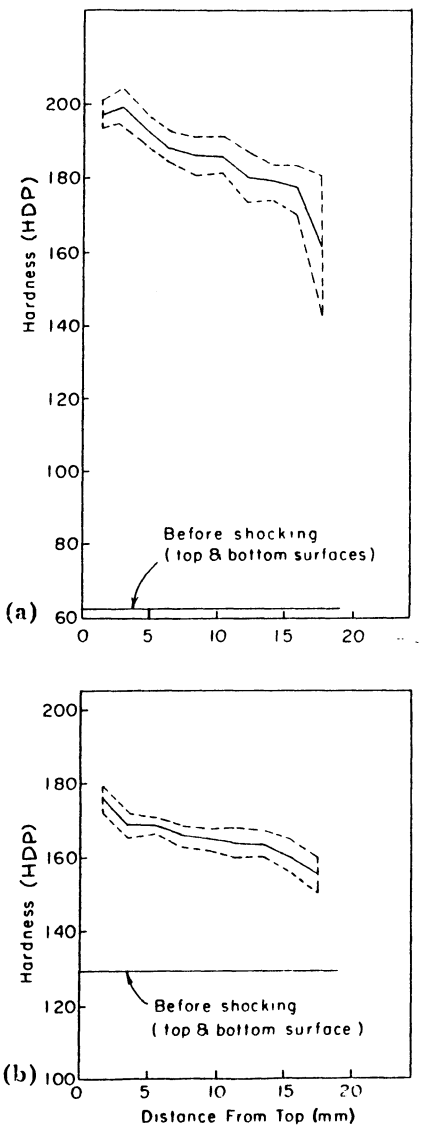

Fig. 3. Hardness as a function of distance from top surface (where the plate impacted the specimens) for (a) an Fe-34.5wt.%Ni bicrystal and (b) an Fe-34.5wt.%Ni polycrystal under a load of 10 kgf (1 HDP = 1 kgf mm^{-2}).

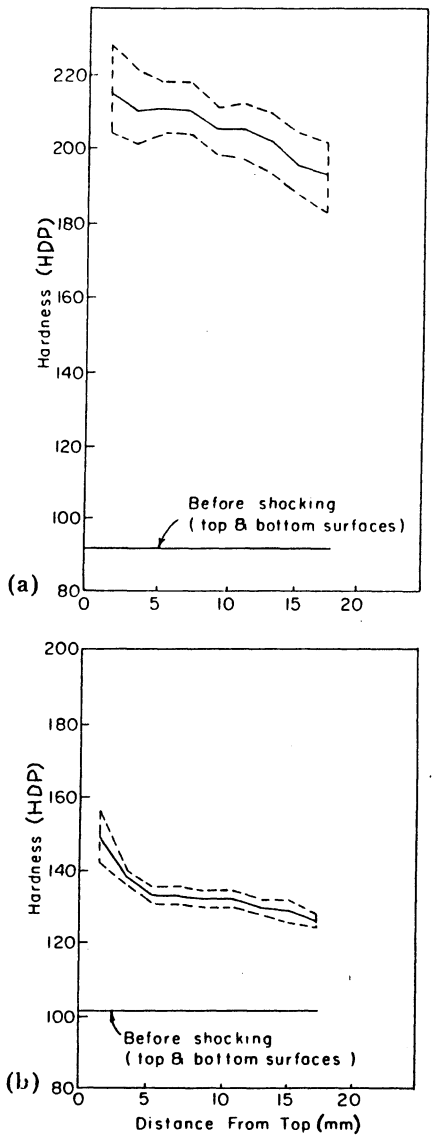

Fig. 4. Hardness as a function of distance from the top surface (where the plate impacted the specimens) for (a) an Fe-15wt.%Cr-15wt.%Ni monocrystal and (b) an Fe-15wt.%Cr-15wt.%Ni polycrystal under a load of 1 kgf (1 HDP = 1 kgf mm^{-2}).

surfaces. The post-shock hardness readings on the top surface are systematically lower than those on the lateral platform closest to the top; this occurs in both monocrystals (or bicrystals) and polycrystals and cannot be an anisotropy effect. It is probably due to the heat generated at the surface during impact, because the surfaces are not perfectly smooth. The large temperature rise induces local recovery, with an attendant decrease in hardness. Urtiew and Grover [15, 16] have shown that these interfacial imperfections can even induce localized melting. Interfacial effects can also take place at the bottom. Hence, the hardness results on the lateral platforms are a more reliable indication of the substructure development. The pre-shock (annealed) hardnesses, however, should be the same for the lateral, top and bottom sides. For this reason, the average hardness between the top and bottom surfaces is shown in the plot as the pre-shock (annealed) hardness for comparison purposes. There is no great difference in the decay rate of the hardnesses for the four conditions, indicating that polycrystallinity does not have a very important effect on the rate of attenuation of the wave. In spite of the fact that the hardnesses of monocrystals were lower than those of the polycrystals prior to shock loading, as expected, the post-shock hardnesses of the single crystals exceed those of the polycrystals substantially. The hardness close to the top surface increased by 40 HDP (from 160 to 200 HDP) for the Fe-34.5wt.%Ni bicrystal, and only by 50 HDP (from 130 to 180 HDP) for the polycrystal. For Fe-15wt.%Cr-15wt.%Ni it increased by 120 HDP (from 90 to 210 HDP) for the monocrystal and by 50 HDP (from 100 to 150 HDP) for the polycrystal. This large difference as well as the consistently higher hardness exhibited by the monocrystals and bicrystals are significant and will be discussed later in connection with the deformation substructure.

The large difference in hardness warranted a closer observation of the impressions left by the indenters. The Fe-34.5wt.%Ni bicrystal exhibits an interesting response after being shocked. The pressure produced by the indenter causes the material to flow upwards. This is shown in Fig. 5, together with the orientation of the plane of the platform determined by Laue back reflection (Fig. 5(a)). The dark regions in Fig. 5(b) surrounding the impression are caused by the extrusion of material. The plastically deformed region exhibits profuse slip markings which were identified as the traces of the {111} slip planes on the plane of the platform. Previous work by Stone [10] did not reveal any deformation twins at ambient temperature after considerable plastic deformation at slow strain rates; for this reason, the markings in Fig. 5 can be considered as being due to slip. In contrast, the hardness indentations made prior to the explosion do not exhibit this response (Fig. 6(b)). The indentation shown was done

TABLE 1

Diamond pyramid hardness prior to and after shocking (5 kgf load)

Material[a]	*Surface*	*Prior to shocking*		*After shocking*	
		Hardness (HDP)	*Standard deviation*	*Hardness* (HDP)	*Standard deviation*
Fe-34.5wt.%Ni BX	Top	60	5.6	145.5	5.6
	Bottom	68.4	3.9	106.8	9.1
Fe-34.5wt.%Ni PX	Top	131.5	4.6	156.4	5.9
	Bottom	129.6	3.4	180	10.1
Fe-15wt.%Cr-15wt.%Ni SX	Top	92.6	12.4	158.5	4.8
	Bottom	94.8	13.7	137.5	10.6
Fe-15wt.%Cr-15wt.%Ni PX	Top	102.2	5.3	127.6	4.9
	Bottom	101.5	3.5	138.6	5.4

[a]SX, single crystal; BX, bicrystal; PX, polycrystal.

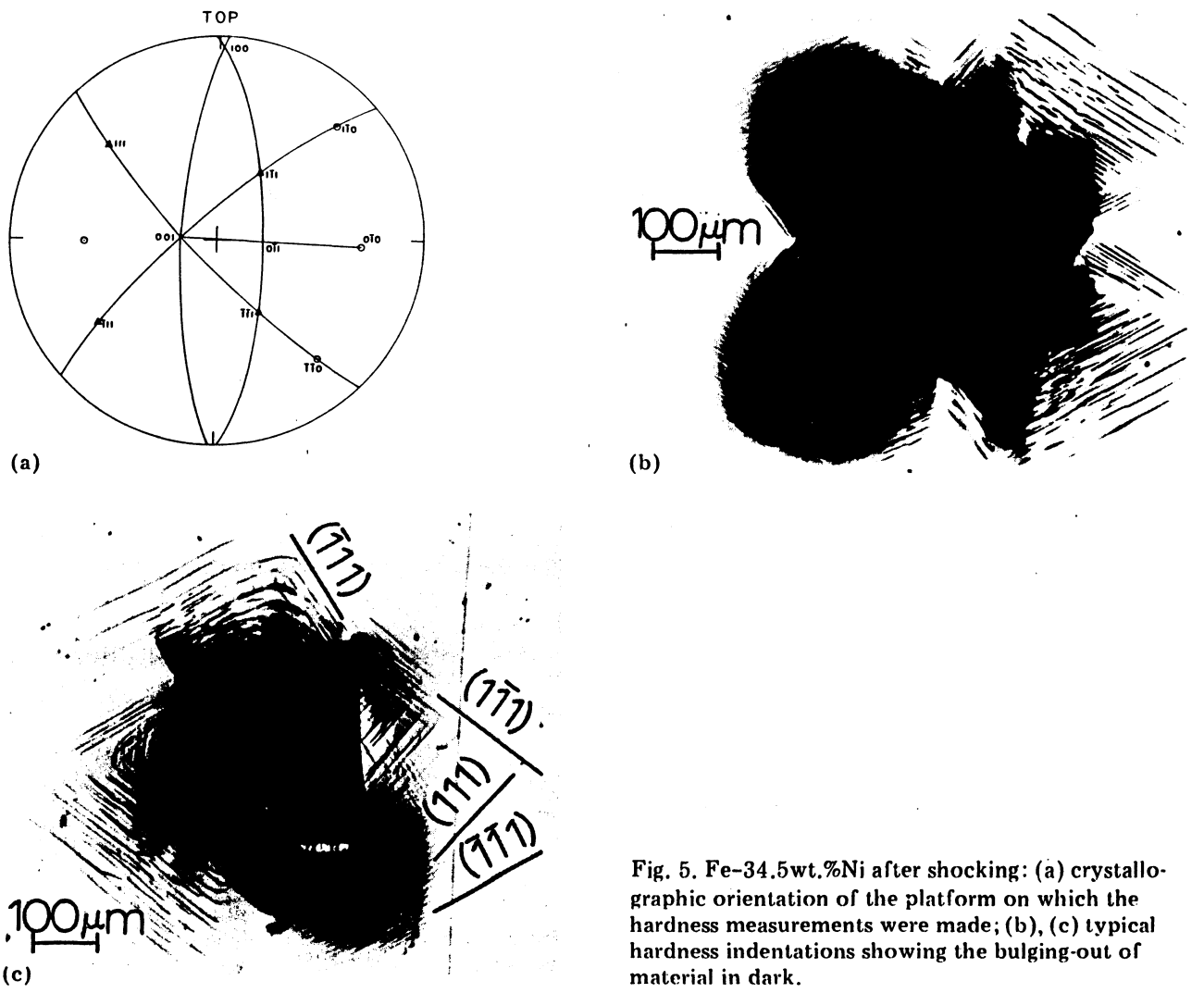

Fig. 5. Fe-34.5wt.%Ni after shocking: (a) crystallographic orientation of the platform on which the hardness measurements were made; (b), (c) typical hardness indentations showing the bulging-out of material in dark.

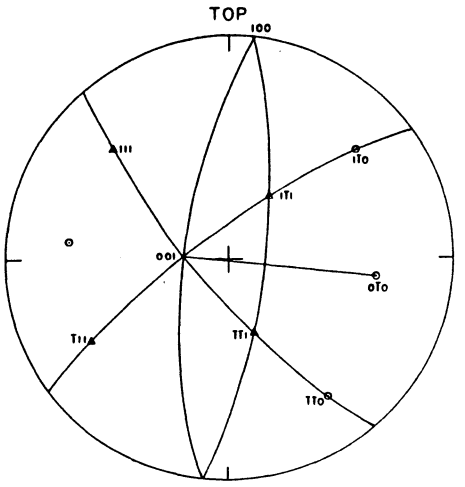

(a)

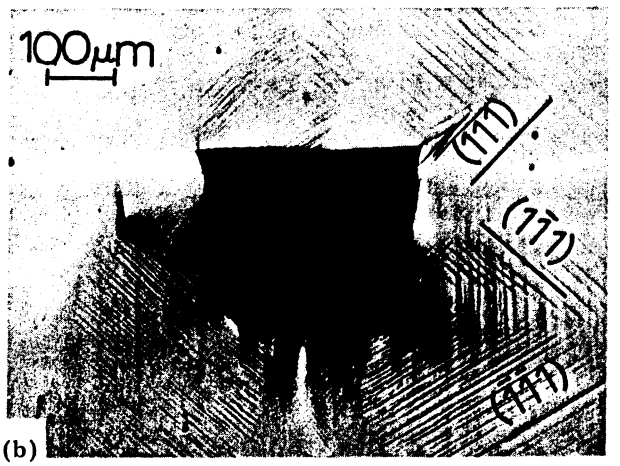

(b)

Fig. 6. Fe-34.5wt.%Ni prior to shocking: (a) crystallographic orientation of the platform on which the hardness measurements were made; (b) typical hardness indentation, with slip markings covering a greater extension than in Figs. 5(b) and 5(c) and without inducing substantial bulging-out.

at a different load from that in Fig. 5(c), because the objective was to generate an indentation of approximately the same size in both specimens. No dark regions are observed, and the slip markings exist over a much larger area, showing that deformation is more uniformly distributed in the material. Pre- and post-shock hardness measurements were made on the same crystallographic planes to allow a true comparison; the hardness of monocrystals has been known to vary with orientation [17]. This can be ascertained from the stereographic projections of Figs. 5(a) and 6(a). The sample was cemented to a goniometer mount and rotated until the same orientation was found.

By comparing the hardness indentations of Figs. 5(b) and 6(b) it can be seen that the slip markings extend over a much wider region in the pre-shock condition. Figure 7 presents a schematic explanation for the differences. The region of plastic deformation has been calculated by the slip line field method (ref. 18, p. 443) for sliding and sticking conditions for an ideally plastic material. Figure 7(a) shows the schematic result for sticking conditions and a metal with constant flow stress (the flow stress is independent of prior deformation). The pyramidal indenter used is the DPH indenter (diamond pyramid or Vickers tests) and it has an apex angle of 136°. Under sticking conditions a region of "dead metal", in which no plastic deformation takes place, precedes the indenter. The lines shown in Fig. 7(a) which are approximately 45° to the surface of the specimen (lines 1, 2, 3 and 4) are the slip lines; they correspond to the planes of maximum shear, along which slip occurs. The states of stress and strain are geometrically similar at any instant of the deformation process; hence, the geometry of the deformation zone is the same and the solution obtained for a certain depth of penetration is applicable to other depths, with the appropriate scale-up or scale-down. Plastic deformation takes place at constant volume

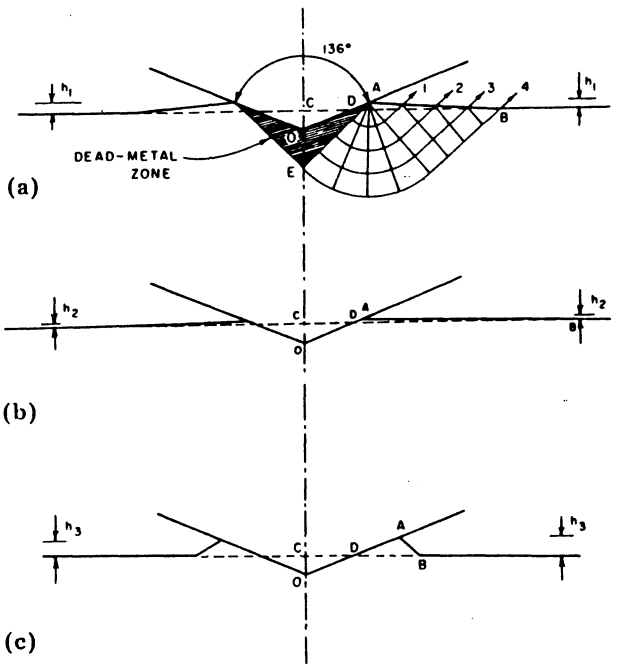

Fig. 7. Schematic representation of the plastic deformation produced by a Vickers (or diamond pyramid hardness) indenter: (a) ideally plastic material, including slip line field; (b) work-hardening material; (c) work-softening material.

and the intrusion produced by the indenter requires an extrusion; hence the volume of the "pile-up" region is equal to the volume displaced by the indenter. In Fig. 7(a),

$$V_{OCD} = V_{DAB} \quad (1)$$

From this geometrical relationship the height h_1 can be calculated. If the material work hardens, the geometry of the pile-up region is different. The flow stress increases with strain, and slip along a certain plane requires increasingly high stresses. Consequently, the slip lines (in the slip line field analysis) are deactivated after a certain amount of deformation. This leads to the accommodation of the deformation in slip planes at regions progressively further away from the indenter zone. In other words, a larger region of dead metal is produced. The situation is depicted in Fig. 7(b). The distance DB is increased, and the requirement of constant volume (eqn. (1)) leads to $h_2 < h_1$. In contrast, work softening should produce the opposite effect. Work softening occurs when the flow stress decreases with plastic deformation; this behavior has been fully characterized by Longo and Reed-Hill [19–21] and has been found to be associated with shock-loaded nickel [22]. As deformation takes place along a slip plane, the flow stress decreases, rendering it increasingly amenable to further deformation. This leads to the localization of plastic deformation. In Fig. 7(c) it can be seen that DB is lower than DB for the ideally plastic case. The constancy of volume requires that $h_3 > h_1$. Hence, it can be concluded that the shape of the pile-up region is related to the plastic response of the material. The analysis above is corroborated by the careful measurements of pile-up profiles made by Böklen [23]. He showed that work-hardened mild steel (exhibiting, thus, a low work-hardening rate) exhibited a pile-up height h twice as large as that of annealed steel (exhibiting a high work-hardening rate). Tabor (ref. 24, p. 15) reports the same effect, describing it as a "piling-up" for highly work-hardened metals and a "sinking-in" for annealed metals. Recent experiments [25] on annealed and shock-loaded nickel showed the same response.

In order to observe the region of deformation under the indentation and to verify the accuracy of the slip line analysis [26], the cross section of a conical hardness indentation produced by a Brale (Rockwell C) indenter was prepared, using an etchant that revealed the slip markings. Figures 8(a) and 8(b) show the results for the annealed and *post explosionem* conditions respectively. The shocked material exhibits pile-up (Fig. 8(b), arrow), while no such feature is observed for the annealed condition. The slip markings seem to be, for the two cases, divided into two groups. They are indicated by 1 and 2 in Fig. 8. Closer to the surface, the slip system 1 is operational, while the slip system 2 is more prominent in the deeper region. Not much can be concluded from these features, except that the slip line field predictions are not obeyed very closely. It should be emphasized, however, that the slip line fields indicate planes of maximum shear stress, while the slip markings of Fig. 8 have to obey the

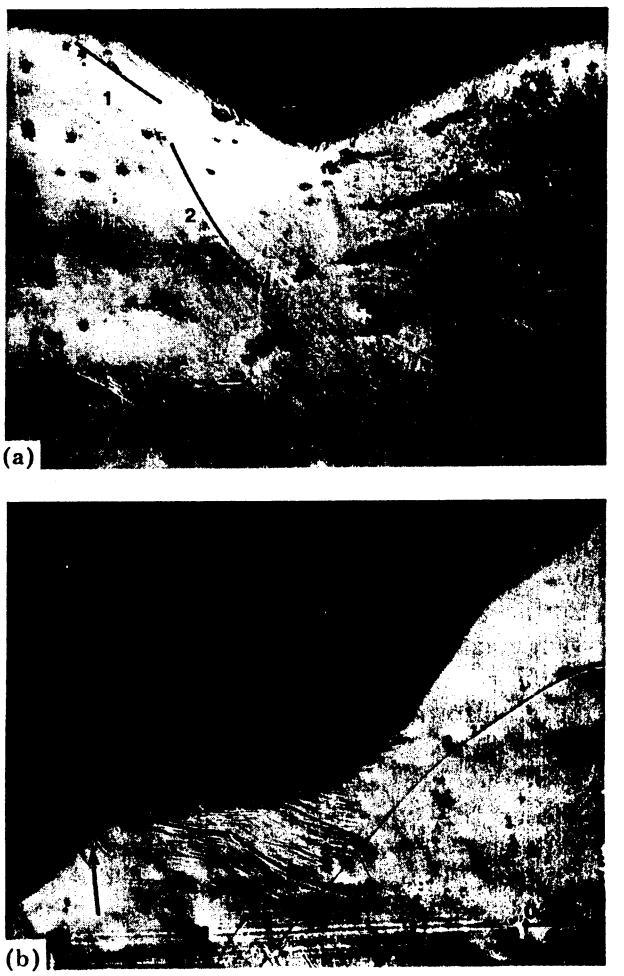

Fig. 8. Cross section of conical indentations in an Fe–34.5wt.%Ni monocrystal, revealing slip markings after etching: (a) annealed condition; (b) *post explosionem* condition.

crystallographic requirements; they are {111} planes. Tabor (ref. 24, p. 47) recommends additional work using metallographic techniques. The slip markings in Fig. 8(b) seem to be more intense and close to the indentation; this is consistent with the piling-up observed in Fig. 5.

These differences in the morphology of hardness indentations indicate that care should be exercised in the analysis of results; cross-comparisons are therefore not very meaningful. To illustrate this, the post-shock hardness of the polycrystalline Fe-34.5wt.%Ni alloy does not exhibit the large bulging (Fig. 9). The deformation in the various grains

Fig. 9. Hardness indentation in an Fe-34.5wt.%Ni polycrystal in a post-shock condition.

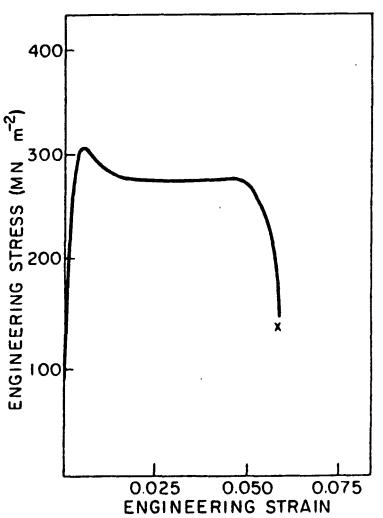

Fig. 10. Engineering stress-engineering strain curve for specimen taken at approximately 2 mm from the top surface of an Fe-34.5wt.%Ni bicrystal in a shocked condition, showing clear evidence of work softening ($\dot{\epsilon} = 2.1 \times 10^{-4}\,s^{-1}$).

can be clearly seen and the plastic strain is accommodated in a rather irregular way around the indentation.

In order to test the hypothesis of work softening, tensile samples were prepared of the post-shock condition. Figure 10 shows that the tensile curve is clearly characteristic of work softening [19-22]. At the yield stress the stress starts dropping; afterwards, there is a plateau, followed by a further stress decrease and fracture. Necking starts at the ultimate stress, which nearly coincides with the yield stress. In structural terms, it is interpreted as follows. At the yield point the substructure generated by shock loading becomes unstable and dislocations start to move. Hence, dislocation rearrangement and no dislocation multiplication occurs, as observed in conventional work hardening. In the stress drop and plateau region the dislocation substructure generated by shock loading is replaced by the substructure characteristic of quasi-static loading at ambient temperature. It will be seen below that the substructure generated by shock loading consists mainly of dislocation tangles and incipient cells. The specimen used in the test presented in Fig. 10 was at a distance of 2 mm from the top surface. Specimens taken from the top disc (about 0.2 mm from surface) did not exhibit the clear work-softening response because the heat generated by impact annealed the substructure and stabilized it.

Since the relationship between the pressure and the size of the indentation remains unchanged whatever the size of the indentation for pyramidal and conical indenters (ref. 24, p. 105), a spherical indenter was used to monitor the progress of work softening. As the sphere penetrates into the metal, the state of strain under it changes because the geometry of the deformation zone is changing. While a mean strain of 0.08 can be defined for the pyramidal indenter (ref. 24, p. 105) (although the strain varies from point to point), the mean strain would increase for a spherical indentation as the penetration proceeds. The progress of deformation can be seen in Fig. 11. The abscissa represents the ratio of the indentation diameter to the sphere diameter; it is a measure of the strain, and Tabor (ref. 24, p. 73) finds that the strain close to the border of the indentation, at the surface, is equal to 20% of the ratio. The ordinate represents the applied load. The

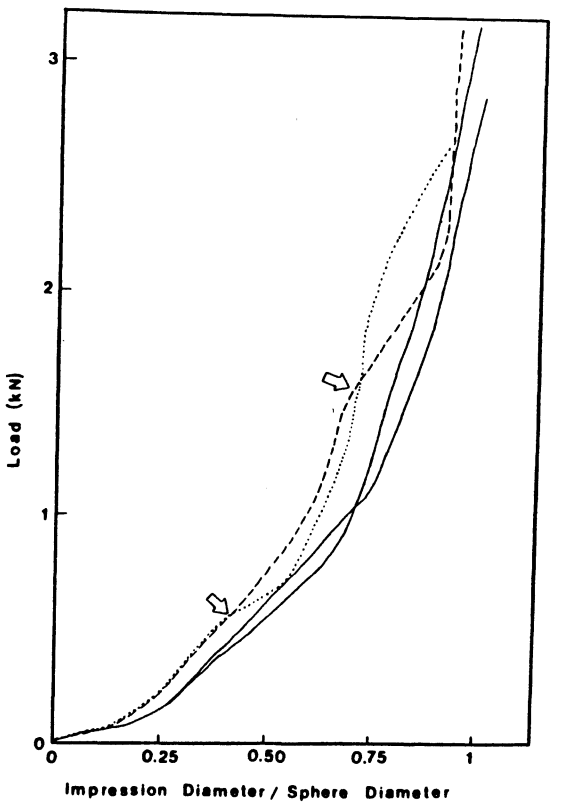

Fig. 11. Load *vs.* indentation diameter divided by sphere diameter for annealed Fe-34.5wt.%Ni (——) and shocked Fe-34.5wt.%Ni (– – –, · · · · ·). The irregularities due to work softening (arrows) should be noted.

annealed condition (full lines) exhibits a response that can be divided into three stages, depending on the value of the ratio: from 0 to 0.25 (small slope), from 0.25 to 0.7 (linear) and from 0.7 to 1 (asymptotically approaching unity). Two different experiments exhibit consistent responses. In contrast, the shocked condition exhibits deviations from the three-stage response. They are marked by arrows in Fig. 11; at a certain strain the metal "softens" and there is a large indentation increase for a relatively small load increase. These two regions, indicated by arrows, corresponded to the concentration of metal pile-up around the indentation. The two experiments exhibited softening at different strains and this is probably because they were made at different distances from the shock impact surface and correspond to regions with different dislocation densities; the indentation closer to the impact surface exhibited softening first (at a ratio of 0.4).

The residual hardness features can be rationalized in some respects by considering the microstructural observations. The dislocation density in the Fe-34wt.%Ni bicrystalline specimens was roughly twice as great as that for the polycrystalline specimens. This was also observed for the Fe-15wt.%Cr-15wt.%Ni single crystals compared with the polycrystalline specimens. In addition, the Fe-15wt.%Cr-15wt.%Ni specimens showed a higher residual dislocation density than the Fe-34wt.%Ni specimens in corresponding categories: single crystals; bicrystals; polycrystals. The difference between the dislocation densities of the Fe-15wt.%Cr-15wt.%Ni and the Fe-34wt.%Ni specimens was that the dislocation density of the former was a factor of 3 greater than that of the latter. This can explain the relative differences in residual microhardness shown in Table 2. Figures 12 and 13 show for comparison the dislocation substructures typical of the shock-loaded samples, where it can be readily observed that there is neither a perceptible nor a measurable difference between the dislocation densities of the top and bottom surface reference, for any category of specimen. Figures 12 and 13 show dislocations imaged under identical operating reflections and the out-of-contrast fraction is identical.

TABLE 2

The average residual dislocation densities and the average differences in hardness

Material[a]	*Average hardness difference (top and bottom) ΔH*	*Average residual dislocation density*[b] (cm^{-2})
Fe-34.5wt.%Ni BX	63	3×10^{10}
Fe-34.5wt.%Ni PX	40	8×10^{9}
Fe-15wt.%Ni-15wt.%Cr SX	55	8×10^{9}
Fe-15wt.%Ni-15wt.%Cr PX	32	3×10^{9}

[a]SX, single crystal; BX, bicrystal; PX, polycrystal.
[b]The dislocation density values are corrected for the out-of-contrast fraction according to the reflection conditions described by Hirsch *et al.* [26].

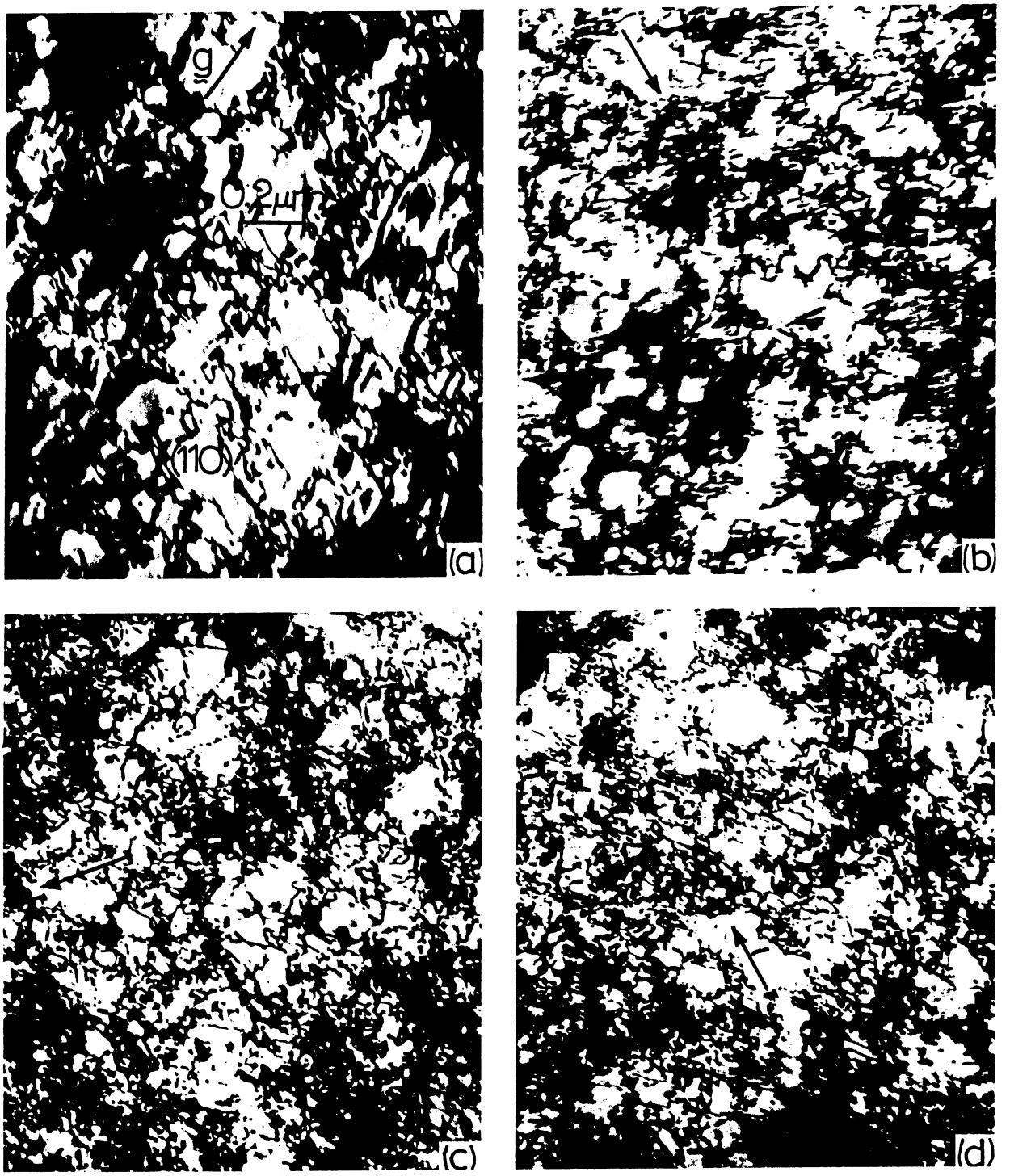

Fig. 12. Transmission electron micrographs of Fe-34.5wt.%Ni (all grains have the same (110) orientation and g// [002] is indicated by arrows in the four micrographs): (a) polycrystal, top; (b) polycrystal, bottom; (c) bicrystal, top; (d) bicrystal, bottom. All magnifications are the same as shown in (a).

In other words, the comparisons are identical except for the fact that surface orientations in Fig. 12 are (110) while those in Fig. 13 are (100). Figure 14(a) shows for comparison with Figs. 12(a) and 13(a) the dislocation image with g// [020]. Figure 14(b), in contrast, shows for comparison with Fig. 12(b) the dislocation structure imaged with g// [$\bar{1}$11].

A comparison of the dislocation substructures in Figs. 12 and 13 shows that the Fe-34wt.%Ni substructures are mainly characterized by poorly formed dislocation cells and

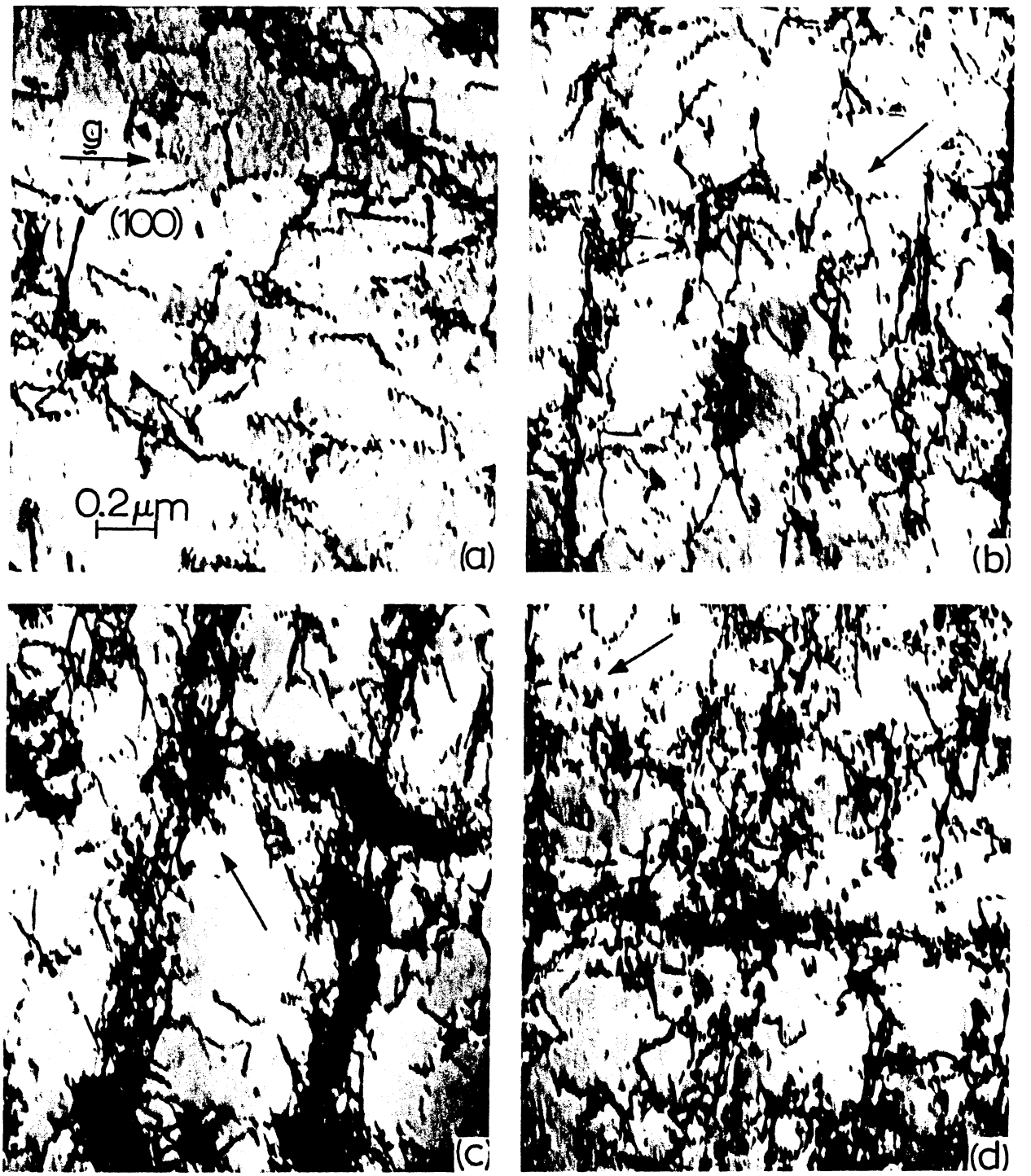

Fig. 13. Transmission electron micrographs of Fe-15wt.%Cr-15wt.%Ni (all grains are (100) and g // [002] is indicated by the arrows in the micrographs): (a) polycrystal, top; (b) polycrystal, bottom; (c) monocrystal, top; (d) monocrystal, bottom. All magnifications are the same as shown in (a).

dislocation tangles while most of the Fe-15wt.%Cr-15wt.%Ni show mainly planar-type dislocation arrays, which are especially prominent in the single-crystal specimens after shock loading. These observations are indicative of a considerably higher dislocation density in the Fe-34wt.%Ni than in the Fe-15wt.%Cr-15wt.%Ni specimens. The stacking fault energy of the Fe-15wt.%Cr-15wt.%Ni alloy can be taken as 30 mJ m^{-2}, from the determinations made by Breedis [27]; in contrast, the Fe-34.5wt.%Ni alloy has a much

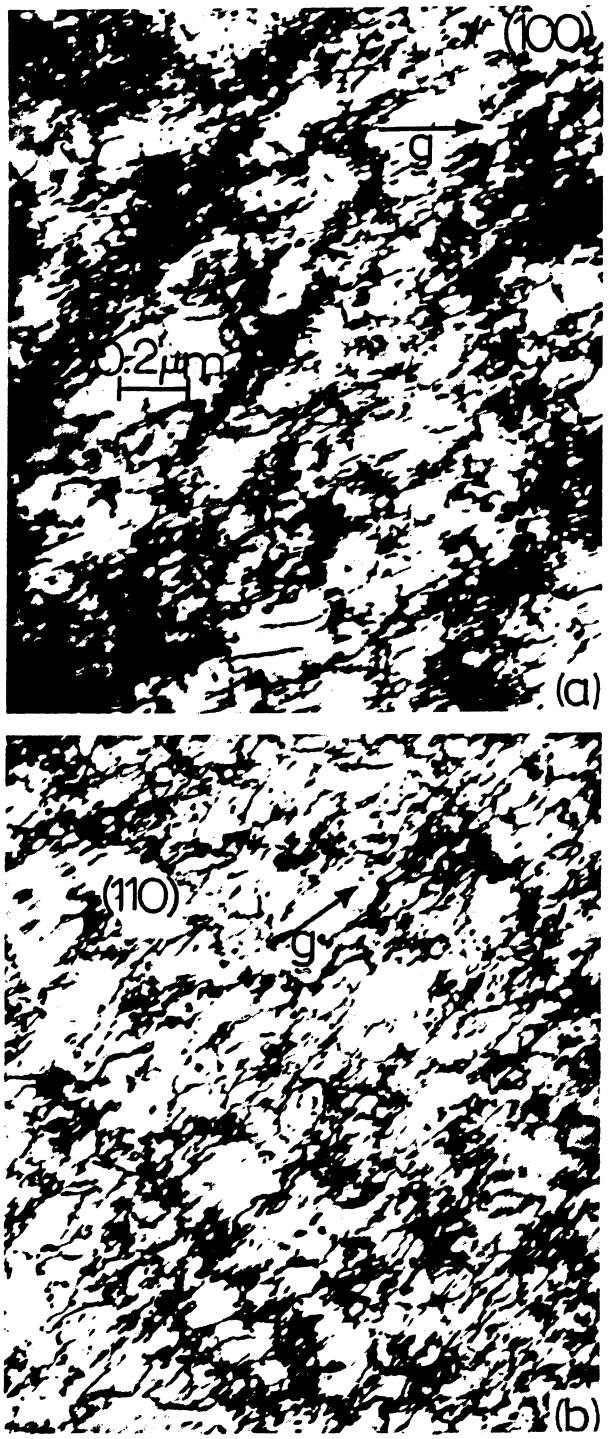

Fig. 14. Fe–34.5wt.%Ni polycrystal: (a) a (100) grain from the top imaged under a [002] operating reflection; (b) a (110) grain from the bottom imaged under a [111] reflection. The magnifications for both images are shown in (a).

higher stacking fault energy. The difference in substructure is consistent with the difference in stacking fault energies.

The fact that dislocation densities are not perceptibly different from the top to the bottom surface reference positions in the polycrystalline specimens of both materials is probably indicative of the fact that the high pressure employed swamped the wavy wave effects which might be important for thicker specimens and lower shock pressures. The experiments provide the first direct evidence of the negligible influence of shock velocity anisotropies at pressures above about 5 GPa.

4. CONCLUSIONS

(a) It is shown that polycrystallinity does not have a noticeable effect on the attenuation of shock waves in the Fe–34wt.%Ni and Fe–15wt.%Cr–15wt.%Ni alloys, at the pressure and within the total depth investigated.

(b) In accordance with the stacking fault energies, the dislocation substructure of shock-loaded Fe–34wt.%Ni was characterized by irregular tangles, while that of Fe–15wt.%Cr–15wt.%Ni consisted of planar dislocation arrays.

(c) The polycrystals exhibited a lower hardness increase than the monocrystals and bicrystals; these hardness increases are consistent with the post-shock dislocation densities.

(d) It is shown that shock loading induced work softening in Fe–34wt.%Ni on subsequent mechanical deformation. This work softening has a strong effect on the deformation produced by the hardness indentations.

ACKNOWLEDGMENTS

This research was partially supported by grants from the Army Research Office (Grant DAAG29-76-G-08181) and the National Science Foundation (Grant DMR-797102).

REFERENCES

1 G. E. Dieter, in J. Hardwood (ed.), *Strengthening Mechanisms*, American Society for Metals, Metals Park, OH, 1962, Chap. 10, p. 279.
2 A. R. Champion and R. W. Rohde, *J. Appl. Phys.*, *41* (1970) 2213.
3 R. N. Orava, M. A. Meyers and G. A. Stone, *Proc. 6th Int. Conf. on High Energy Rate Fabrication, Essen, September 1977*, p. 5.2.1.
4 H.-J. Kestenbach and M. A. Meyers, *Metall. Trans. A*, *7* (1976) 1943.
5 K. Wongwiwat and L. E. Murr, *Mater. Sci. Eng.*, *35* (1978) 273.

6 L. E. Murr, H. R. Vydyanath and J. V. Foltz, *Metall. Trans., 1* (1970) 3215.
7 J. R. Rempel, D. N. Schmidt, J. O. Erkman and W. M. Isbell, *Tech. Rep. W1-Tr-65-119*, February 1966 (Stanford Research Institute) (Air Force Weapons Laboratory Contract AF 29(601)-6040).
8 J. O. Erkman and A. B. Christensen, *J. Appl. Phys., 38* (1967) 5395.
9 M. A. Meyers and M. S. Carvalho, *Mater. Sci. Eng., 24* (1976) 131.
10 G. A. Stone, *M.Sc. Thesis*, University of California, Berkeley, 1971; *LBL Rep. 134*, 1971 (Lawrence Berkeley Laboratory).
11 G. A. Stone, *Ph.D. Thesis*, University of California, Berkeley, 1974; *LBL Rep. 1800*, 1974 (Lawrence Berkeley Laboratory).
12 G. A. Stone and G. Thomas, *Metall. Trans. A, 5* (1974) 2095.
13 P. S. deCarli and M. A. Meyers, in M. A. Meyers and L. E. Murr (eds.), *Shock Waves and High-strain-rate Phenomena in Metals: Concepts and Applications*, Plenum, New York, 1981, p. 341.
14 R. Kinslow (ed.), *High-velocity Impact Phenomena*, Academic Press, New York, 1970, p. 551.
15 P. A. Urtiew and R. Grover, *J. Appl. Phys., 45* (1974) 140.
16 R. Grover and P. A. Urtiew, *J. Appl. Phys., 45* (1974) 146.
17 D. Lee, in J. H. Westbrook and H. Conrad (eds.), *The Science of Hardness Testing and its Research Applications*, American Society for Metals, Metals Park, OH, 1973, p. 147.
18 M. C. Shaw, in F. A. McClintock and A. S. Argon (eds.), *Mechanical Behavior of Materials*, Addison-Wesley, Reading, MA, 1966, Chap. 13.
19 W. P. Longo and R. E. Reed-Hill, *Scr. Metall., 4* (1970) 765.
20 W. P. Longo and R. E. Reed-Hill, *Scr. Metall., 6* (1972) 833.
21 W. P. Longo and R. E. Reed-Hill, *Metallography, 4* (1974) 181.
22 M. A. Meyers, *Metall. Trans. A, 8* (1977) 1581.
23 R. Böklen, in J. H. Westbrook and H. Conrad (eds.), *The Science of Hardness Testing and its Research Applications*, American Society for Metals, Metals Park, OH, 1973, p. 109.
24 B. Tabor, *The Hardness of Metals*, Clarendon, Oxford, 1951.
25 K. C. Hsu and M. A. Meyers, New Mexico Institute of Mining and Technology, unpublished results, 1981.
26 P. Hirsch, A. Howie, R. B. Nicholson, D. W. Pashley and M. J. Wheelan, *Electron Microscopy of Thin Crystals*, R. E. Krieger, Huntington, NY, 1977, p. 423.
27 J. F. Breedis, *Trans. AIME, 230* (1964) 1583.